Journal of Catalysis 279 (2011) 205–212

Contents lists available at ScienceDirect

Journal of Catalysis

journal homepage: www.elsevier.com/locate/jcat

Generation of organic radicals during photocatalytic reactions on TiO_2

M.A. Henderson *, N.A. Deskins [1], R.T. Zehr, M. Dupuis

Institute for Interfacial Catalysis, Pacific Northwest National Laboratory, P.O. Box 999, MS K8-87, Richland, WA 99352, United States

ARTICLE INFO

Article history:
Received 22 October 2010
Revised 18 January 2011
Accepted 20 January 2011
Available online 24 February 2011

Keywords:
Photocatalysis
TiO_2
Surface
Radicals
Photodesorption
DFT
Theory

ABSTRACT

Using a variety of organic carbonyl molecules ($R_1C(O)R_2$) and the rutile TiO_2(1 1 0) surface as a model photocatalyst, we demonstrate both experimentally and theoretically that ejection of organic radicals from TiO_2 surfaces is likely a prevalent reaction process occurring during heterogeneous photooxidation of organic molecules. Organic carbonyls react with coadsorbed oxygen species to form organic diolates which are more strongly bound to TiO_2 than are the parent carbonyls. The parent carbonyls, when bound to TiO_2(1 1 0) in an η^1 configuration, are photo-inactive toward valence band holes. However, the diolates are shown to photodecompose by ejection of one of the two R substituents from the surface into the gas phase, leaving behind the carboxylate of the other R group. Theoretical calculations using DFT show that in most cases the choice of which R group is ejected can be predicted based on the C–R bond energies and, to a lesser extent, the stability of the ejected R group.

© 2011 Elsevier Inc. All rights reserved.

1. Introduction

Heterogeneous photocatalysis relies on photogenerated electron–hole pairs to accomplish chemical transformation via surface redox reactions. Under applied conditions, these redox reactions are generally accomplished with a media above the photocatalyst surface. This media, typically in the form of an aqueous or gaseous environment, plays direct (e.g., supplying reactants) or indirect (e.g., assisting in transporting reactants and products away from the surface) roles in photocatalytic processes, but it can also hinder the researcher's ability to detect transient and reactive species generated as a result of charge transfer at the photocatalyst surface. Generation of organic radicals should come as no surprise since the redox steps associated with organic photooxidation are essentially single electron transfer events. There is ample EPR evidence in the photocatalysis literature for the production of organic radicals in indirect (O_2^- mediated) reaction processes [1–5]; however, evidence for production of radicals by direct (hole-mediated) processes has been more elusive. Transient and reactive species resulting from charge transfer events occurring in the pores of high surface area photocatalysts can go undetected because these species invariably encounter other surfaces or other species, and react before they can be detected. Perhaps a good example of this is the photooxidation of 2-propanol to acetone, which requires two oxidation events but for which the intermediate(s) are not observed under typical reaction conditions [6–14]. Studies on single crystal TiO_2 in ultrahigh vacuum (UHV) afford an opportunity to detect events associated with desorption of reactive species, such as radicals, that result from charge transfer events at TiO_2 surfaces. In this study, we provide experimental and theoretical data illustrating the important role that organic radicals play in charge transfer events at TiO_2 surfaces by examining radicals generated through single electron transfer events during the photodecomposition of various organic carbonyl molecules on the rutile TiO_2(1 1 0) surface under UHV conditions.

2. Methods

A rutile TiO_2(1 1 0) crystal was employed as a model TiO_2 photocatalyst surface. Details of preparation of this surface for photochemical studies and on the UHV system used in this study can be found elsewhere [15]. Surface cleaning consisted of sputter/anneal cycles. Research grade reagents were dosed onto the TiO_2(1 1 0) surface using a molecular beam dosing system, and gas lines were passivated by exposure to the specific gas for several hours before first use. Photodesorption and TPD signals were both collected in line-of-sight geometries between the TiO_2(1 1 0) surface and the mass spectrometer. Photon exposures were accomplished using a 100-W Hg arc lamp. Light was focused from the lamp onto a fused silica fiber optic light delivery system and brought to the sample through a fiber optic feedthrough. Typical UV fluxes were $\sim 2.0 \times 10^{16}$ photons/cm^2 s. Little or no temperature rise was registered at the crystal during UV irradiation.

* Corresponding author.
E-mail address: ma.henderson@pnl.gov (M.A. Henderson).
[1] Present address: Department of Chemical Engineering, Worcester Polytechnic Institute, 100 Institute Road, Worcester, MA 01609-2280, United States.

0021-9517/$ - see front matter © 2011 Elsevier Inc. All rights reserved.
doi:10.1016/j.jcat.2011.01.021

Surfaces with coadsorbed organic carbonyl and oxygen were prepared by exposing the surface to 20 L O_2 at 95 K (1 L = 1×10^{-6} torr s) followed by dosing excess organic at 95 K. The surface was then heated to above 200 K to complete the reaction of the organic with oxygen to form the photoactive diolate species. This process also desorbed excess (photo-inactive) organic.

Density functional theory (DFT) simulations were performed on the rutile TiO_2(1 1 0) surface in the presence of various organic molecules. Accurate chemical energies and geometries are obtainable using this method, and catalytic processes are readily treated. The DFT simulations give structures at 0 K and therefore ignore temperature effects. Nevertheless, the energetics of surface processes is key (if not the controlling factor in many cases) and therefore DFT provides useful information on the relevant surface chemistry. We used a slab model to describe the surface, wherein a portion of the surface was set in a simulation cell and subjected to periodic boundary conditions. An empty space, or vacuum, existed above and below the slab. Our slab consisted of a (4×2) surface cell that was four layers thick (12 atomic layers). In the current work, we modeled adsorption of several organic carbonyls over clean stoichiometric surfaces, and over surfaces with adsorbed O adatoms (O_a). All calculations were performed with the CP2K package [16–18] using the PBE exchange correlation functional [19]. The valence electrons were treated by a dual basis, with wavefunctions represented by Gaussian functions, while the electron density was represented by plane waves. Double-zeta Gaussian functions were used, and the plane waves were expanded up to 300 Rydberg. Core electrons were represented by pseudopotentials [20,21]. Further details of the computational methodology are found in the Supplementary information.

3. Results and discussion

3.1. Adsorption and thermal chemistry

Fig. 1 shows a schematic illustration of the combined thermal and photochemical reaction mechanism for photodecomposition of organic carbonyl molecules on the rutile TiO_2(1 1 0) surface. The basis for this reaction scheme comes from extensive studies on acetone adsorbed on TiO_2(1 1 0) [15,22–24] and from supporting studies on butanone [25], acetaldehyde [26], trifluoroacetone [27], hexafluoroacetone [28] and a variety of other molecules [29]. These examples show that this two-step reaction scheme can be extended to many other organic carbonyls. In the first step, organic carbonyl molecules adsorbed on the TiO_2(1 1 0) surface in an η^1 configuration react with coadsorbed oxygen to form η^2 (bridging) diolate species. Reduced surface cation sites (Ti^{3+}), generated thermally or by trapping of photoexcited electrons, are needed to adsorb oxygen. Vibrational spectroscopy and isotopic labeling studies have both shown that acetone reacts with adsorbed O_a species [30,31] on the TiO_2(1 1 0) surface to generate the acetone diolate species [15,22–24]. DFT calculations also show that the diolate structure represents an energetically stable configuration for organic carbonyls on TiO_2(1 1 0). Fig. 2 shows structures and adsorption energies for acetone bound in three possible configurations on the TiO_2(1 1 0) surface. The η^1 configuration, shown at the top of Fig. 2, is a common bonding structure for adsorbed acetone on oxides and metals. DFT estimates an adsorption energy of −72 kJ/mol for the η^1 configuration, which is comparable but slightly less than that estimated with TPD for acetone on TiO_2(1 1 0) [22]. DFT shows that the η^1 configuration is considerably more stable than the next most stable configuration on the 'clean' surface, that being where a bridging O^{2-} site is permitted to coordinate with the carbonyl C atom (middle of

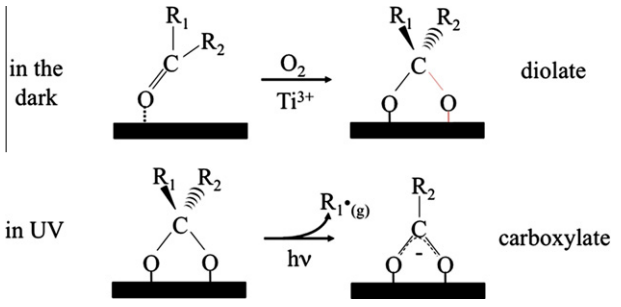

Fig. 1. General reaction scheme for photodecomposition of organic carbonyl molecules on the TiO_2(1 1 0) surface.

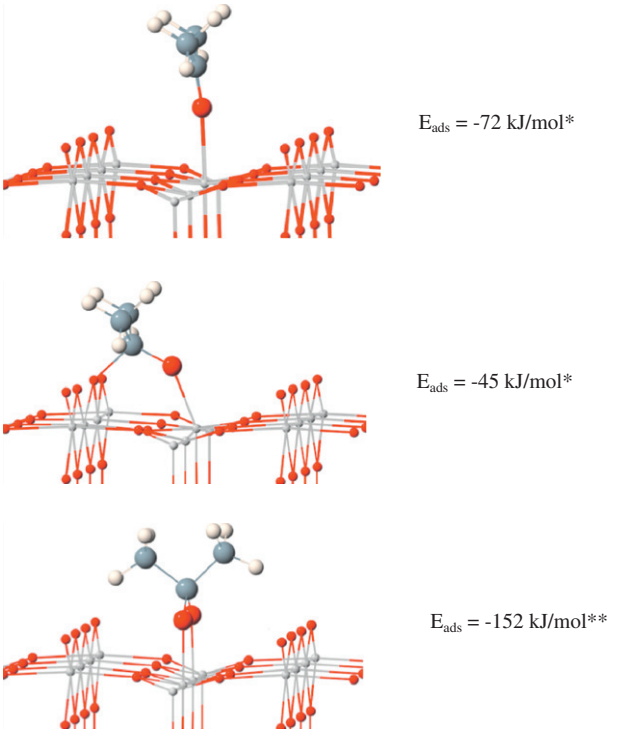

Fig. 2. Structures and adsorption energies derived from DFT calculations for η^1-bound acetone (top), for η^2-bound acetone where the carbonyl carbon atom is coordinated to a bridging O^{2-} site (middle), and for η^2-bound acetone diolate (bottom). (*Energy is relative to the clean surface; **energy is relative to the clean surface with an oxygen adatom bound to a 5-coordinate Ti^{4+} site.)

Table 1
DFT energies for adsorption of various gaseous organic carbonyls on TiO_2(1 1 0) in η^1 configurations with the molecular plane parallel (||) and perpendicular (⊥) to the cation row direction, and for the same gaseous organic carbonyls reacting with an adsorbed oxygen adatom to form an adsorbed organic diolate. All values in kJ/mol.

Parent carbonyl	η^1 state ||/⊥	Diolate state
Acetone	−74/−81	−152
Acetaldehyde	−68/−69	−170
2-Butanone	−63/−64	−155
Pinacolone[a]	−62/−62	?
Acetophenone	−72/−77	−130
Acetyl chloride	−54/−54	−90
1-Chloroacetone	−61/−73	−159
1,1-Dichloroacetone	−55/−69	−149
1,1,1-Trichloroacetone	−52/−44	−90
1,1,1-Trifluoroacetone	−54/−40	−132
Hexafluoroacetone	−26/−11	−96

[a] A bound state for this diolate species was not found with DFT.

Fig. 2). This latter structure may also occur for acetone adsorption at step edges, although this hypothesis is not explored here.

Molecular oxygen dissociates at oxygen vacancy sites on TiO_2(1 1 0) to fill the vacancies and generate O_a species bound at a neighboring 5-coordinate Ti^{4+} sites [30–33]. Dissociation processes yielding O_a species have also recently been discovered that involve non-vacancy sites [34,35]. With O_a present on the TiO_2(1 1 0) surface, the adsorption energy of acetone in an η^2 diolate configuration (bottom of Fig. 2) is roughly twice as stable as that of the η^1 configuration (top of Fig. 2). Table 1 presents adsorption energies obtained from DFT for various organic carbonyls bound on the TiO_2(1 1 0) surface in the η^1 configuration (Reaction 1 for acetone) and as diolates from reaction with O_a (Reaction 2 for acetone).

$$\text{acetone}_{(g)} \rightarrow \eta^1\text{-acetone}_{(a)} \quad (1)$$

$$\text{acetone}_{(g)} + O_{(a)} \rightarrow \text{acetone diolate}_{(a)} \quad (2)$$

In the η^1 case, the molecular plane of the carbonyl can be either parallel (||) or perpendicular ($\perp$) to the direction of the rows on TiO_2(1 1 0). The calculations show that the perpendicular orientation of the η^1 adsorption state is slightly preferred in the cases of acetone, acetophenone, chloroacetone, and dichloroacetone, but the parallel orientation is preferred for the highly halogenated acetones, with no significant preference for the other molecules. Destabilization of the perpendicular η^1 orientation for the highly halogenated acetones is attributed to repulsions between halogens (on the tri-halogenated groups) and bridging O^{2-} sites. DFT calculations (Table 1) also show that favorable adsorption energies are achieved for these organic carbonyl molecules on TiO_2(1 1 0) as diolates. With the exception of the case of pinacolone, the differences between the diolate adsorption energies and the η^1 adsorption energies ranged from −36 kJ/mol in the case of acetyl chloride to between −90 and −100 kJ/mol in the cases of acetaldehyde, 2-butanone, chloroacetone, dichloroacetone, and trichloroacetone.

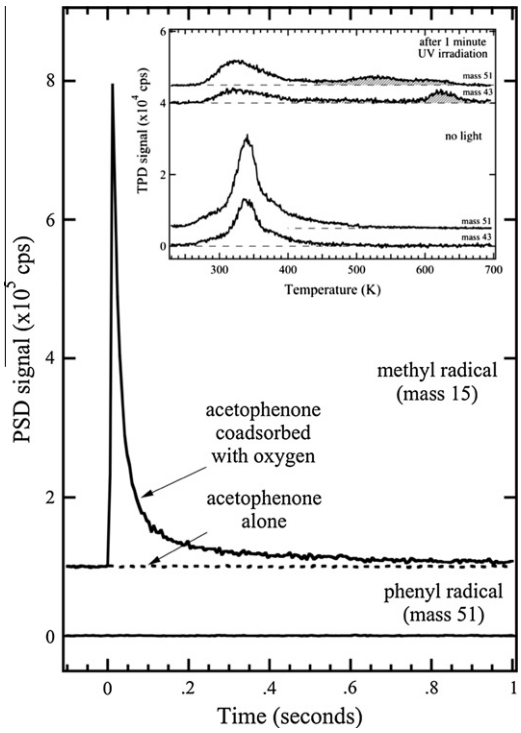

Fig. 4. Photodesorption signals for methyl radical at mass 15 (CH_3^+) and for phenyl-containing species at mass 51 ($C_4H_3^+$) for photodecomposition of acetophenone diolate (from coadsorption of acetophenone and oxygen) on TiO_2(1 1 0). The case for mass 15 from acetophenone alone (no oxygen) is also shown as a dashed trace. Inset: TPD spectra of acetophenone for masses 43 and 51 with (top) and without (bottom) UV irradiation.

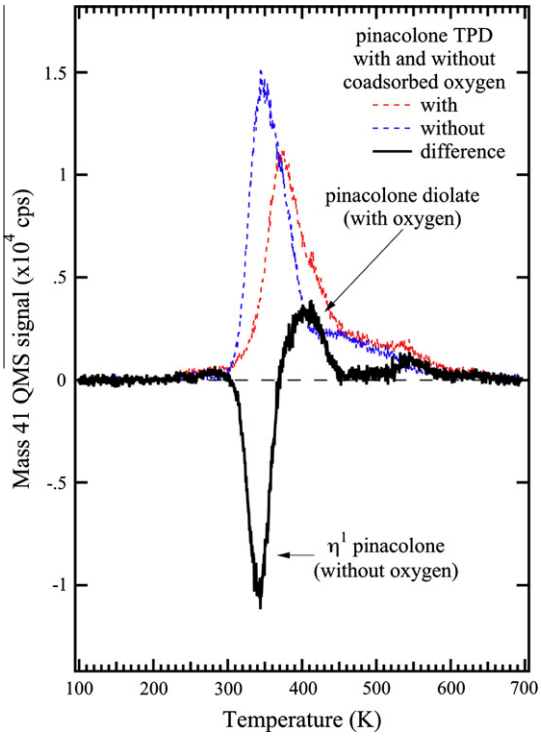

Fig. 3. Mass 41 TPD spectra from a submonolayer coverage of pinacolone on TiO_2(1 1 0) with (dashed red trace) and without (dashed blue trace) coadsorbed oxygen. The difference spectrum of these two experiments is shown in black. (For interpretation of the references to color in this figure legend, the reader is referred to the web version of this article.)

The results in Table 1 suggest that generally speaking, the diolate structure should be energetically more favorable for organic carbonyls adsorbed on TiO_2(1 1 0) than for the η^1 configuration, and that the latter should react to form the former if O_a species are available. This conclusion is supported by TPD results for various organic molecules that show carbonyl desorption from the η^1 state occurring at lower temperatures than from the diolate state [15,22–28]. These results suggest that adsorbed species of this structure may be important surface species in the catalysis and photocatalysis of organic carbonyl molecules on TiO_2 surfaces. The DFT results for pinacolone appear an exception to this assertion. TPD results show that pinacolone ($CH_3C(O)C(CH_3)_3$) is stabilized on TiO_2(1 1 0) when coadsorbed with oxygen (Fig. 3), consistent with the behavior of other carbonyls when coadsorbed with oxygen. In the absence of coadsorbed oxygen, a submonolayer coverage of pinacolone desorbed with a TPD peak at 350 K, with an additional lower coverage state at ~450 K assigned to desorption from step edges. Adsorption of a similar coverage on the oxygen pretreated surface resulted in a shift of the pinacolone TPD peak to 400 K and a depletion of signal at lower desorption temperatures. This shift is illustrated in the difference spectrum (solid trace). The desorption intensity shifted to higher temperature is assigned to thermal decomposition of the pinacolone diolate, a process that liberates back gaseous pinacolone and leaves O_a on the surface. The DFT results however indicate that diolates of these species are not stable, leading to radical ejection and formation of a surface carboxylate. In the pinacolone case, it is ejection of a *t*-butyl radical. More on this ejection process for the diolates will be discussed in the next section.

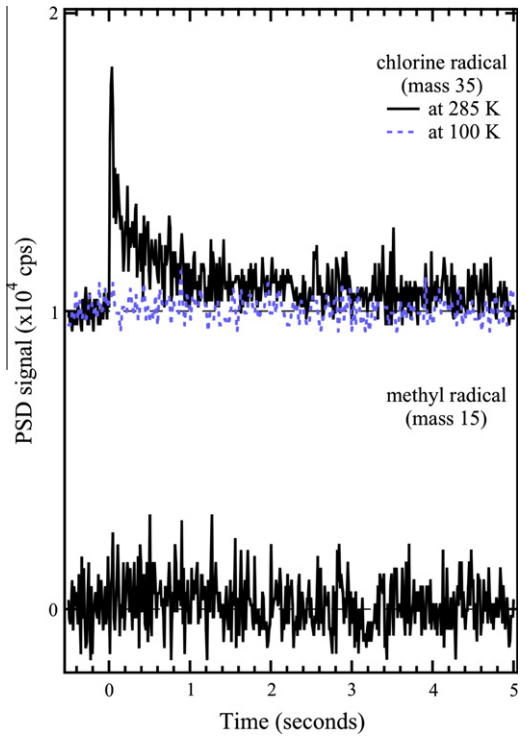

Fig. 5. Photodesorption signals for methyl radical at mass 15 (CH_3^+) and for chlorine radical at mass 35 (Cl^+) for photodecomposition of acetyl chloride diolate on TiO_2(1 1 0). Black traces are with the surface held at 285 K, and the dashed blue trace is for mass 35 with the surface held at 100 K. (For interpretation of the references to color in this figure legend, the reader is referred to the web version of this article.)

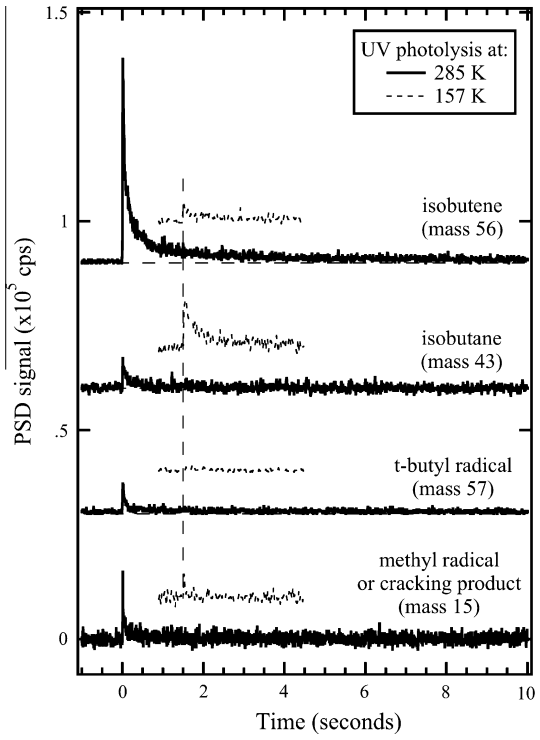

Fig. 6. Photodesorption signals at mass 15 (CH_3^+), 43 ($C_3H_7^+$), 56 ($C_4H_8^+$) and 57 ($C_4H_9^+$) for photodecomposition of pinacolone diolate on TiO_2(1 1 0). Solid and dashed traces are for UV irradiation with the sample at 285 and 157 K, respectively. Traces for the latter are displaced for ease of viewing with a vertical dashed line marking the onset of UV irradiation.

3.2. Charge transfer chemistry

The η^1 configuration of adsorbed organic carbonyls on TiO_2(1 1 0) is not photoactive by means of a hole-mediated process. Achieving photoactivity requires conversion of these species to the diolate structure (with coadsorbed oxygen). The absence of photoactivity for η^1-acetone [15], η^1-trifluoroacetone [27], and η^1-hexafluoroacetone [28] on clean TiO_2(1 1 0) has been demonstrated previously. The explanation for an absence of photochemistry for organic carbonyls in the η^1 configuration is likely due to poor overlap between a valence band hole in TiO_2 and valence electrons on these adsorbed species. Fig. 4 illustrates the photoinactivity of acetophenone on clean TiO_2(1 1 0) in the absence of coadsorbed oxygen. No photodesorption is detected during irradiation of acetophenone alone (e.g., see dashed trace for mass 15), and no decomposition products were detected in post-irradiation TPD (inset of Fig. 4). However, a sharp mass 15 photodesorption spike was seen when the acetophenone diolate species (formed from coadsorption of acetophenone and oxygen) was irradiated with UV (which commenced at time '0' seconds). Evidence of photoactivity was also seen in post-irradiation TPD (inset) in terms of both the depletion of acetophenone TPD signals (compare amounts in the mass 43/51 channels below 400 K with and without UV irradiation) and the presence of decomposition products at higher temperatures. These results demonstrate that the acetophenone diolate readily decomposes on UV irradiation through a process that ejects a methyl radical into the gas phase and leaves organic species (e.g., benzoate) on the surface. The contrasting process would involve ejection of a phenyl radical into the gas phase and retention of acetate on the surface. However, no photodesorption signal was seen at any mass that would indicate ejection of phenyl or phenyl-containing species (e.g., no mass 51 signal as shown in Fig. 4). As implied in the schematic illustration of Fig. 1, the photochemistry that leads to desorption of radicals results from breaking of the bond between the carbonyl C and one of the carbonyl substituents ('R_1' in Fig. 1) and retention on the surface of a carboxylate with the other carbonyl substituent ('R_2' in Fig. 1). In the acetophenone case, data in Fig. 4 indicate that the C–CH_3 bond is broken exclusively, and the C–C_6H_5 bond is retained on the surface.

It is important to determine what factors decide which bond (if any) is broken in cases where $R_1 \neq R_2$. Many combinations of R_1 and R_2 substituents in the reaction scheme of Fig. 1 could be explored in an effort to address this issue; however, it is helpful to keep one of these constant (e.g., as methyl) and vary the other. As mentioned earlier, we have published examples in the cases of acetaldehyde [26], butanone [25], and trifluoroacetone [27] showing selectivity and/or partitioning between photochemical channels of the associated diolates on TiO_2(1 1 0). Fig. 4 has provided a fresh example in the form of acetophenone and oxygen coadsorbed on TiO_2(1 1 0). Additional examples of the diolate photodecomposition mechanism leading to desorbed radicals are presented in Figs. 5–8 for acetyl chloride, pinacolone, and mono-, di- and tri-chloroacetones. Photodesorption data for the acetyl chloride case are shown in Fig. 5. UV irradiation of coadsorbed acetyl chloride and oxygen at 100 K yielded no signal in either the chlorine (dashed trace) or methyl (not shown) desorption channels. However, a similar experiment with the sample held at 285 K (solid traces) clearly showed photodesorption of Cl (mass 35) but not methyl (mass 15). The difference between the 100 and 285 K examples is attributed to the inability of photodesorbing Cl to escape the surface at the lower temperature.

Fig. 6 provides evidence for photochemistry in the case of coadsorbed pinacolone and oxygen. At 285 K, substantial photodesorption resulted from UV irradiation of coadsorbed pinacolone and

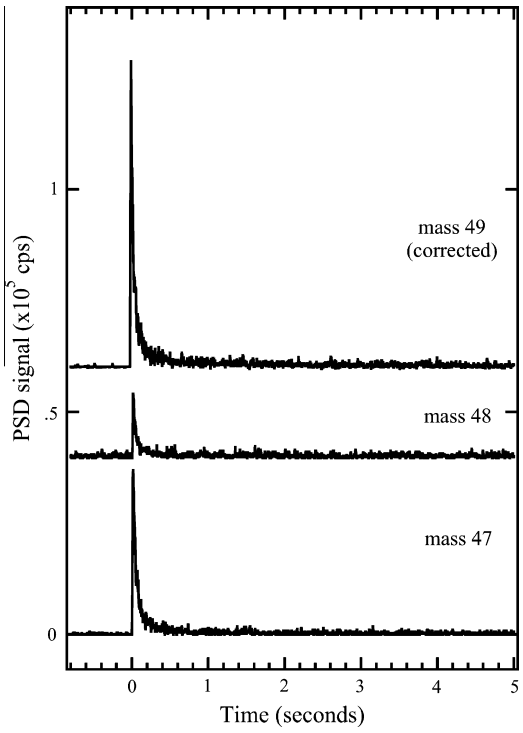

Fig. 7. Photodesorption signals for chloromethyl radical (CH_2Cl) at mass 47 ($C^{35}Cl^+$), mass 48 ($CH^{35}Cl^+$) and mass 49 ($CH_2^{35}Cl^+$) from photodecomposition of chloroacetone diolate on TiO_2(1 1 0). The $C^{37}Cl^+$ contribution was removed from the mass 49 trace.

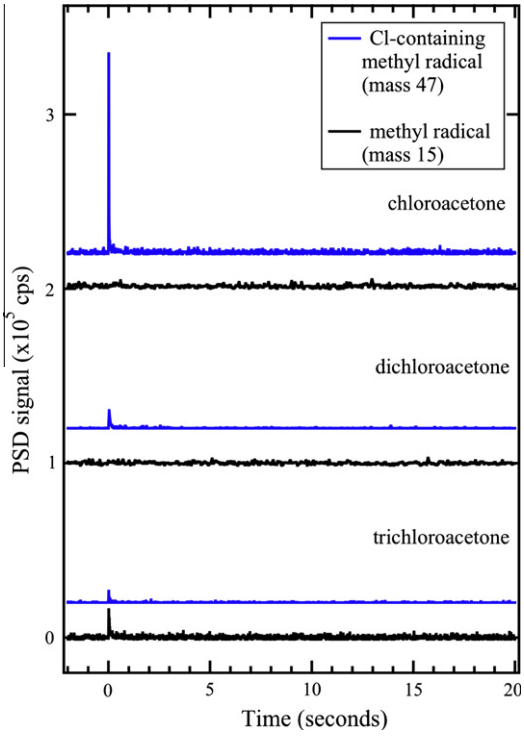

Fig. 8. Photodesorption signals for methyl radical (mass 15, black traces) and Cl-containing methyl radical (using mass 47, blue traces) options for photodecomposition of adsorbed diolates made from (top) chloroacetone ($CH_3C(O)CH_2Cl$), (middle) dichloroacetone ($CH_3C(O)CHCl_2$), and (bottom) trichloroacetone ($CH_3C(O)CCl_3$). (For interpretation of the references to color in this figure legend, the reader is referred to the web version of this article.)

oxygen on TiO_2(1 1 0). (Note that based on data in Fig. 3, the pinacolone diolate should be stable on TiO_2(1 1 0) up to ~350 K.) The main photodesorption signals were at masses 15, 43, 56, and 57, although signals detected at other masses indicated significant mass spectrometer cracking of the main photodesorption products. The mass 43, 56, and 57 signals have been shown to selectively reflect isobutane, isobutene, and *t*-butyl radical, respectively [36], whereas signals from other masses (e.g., mass 39 and 41) have contributions from more than one of these photodesorbing species. No photodesorption signal was detected that could be attributed to any product other than these three. Although not normalized for relative mass spectrometer cracking efficiencies, the data in Fig. 6 indicate that the primary product photodesorbing during UV irradiation of pinacolone diolate on TiO_2(1 1 0) was isobutene. This molecule resulted from an ejected *t*-butyl radical depositing an H-atom on the surface. Weaker signals at mass 43 and 57 resulted from *t*-butyl radicals that picked up an H-atom (from the isobutene production channel) to form isobutane or that escaped the surface intact, respectively. The mass 15 signal shown in Fig. 6 may have resulted from one of two sources: photodesorption of methyl radicals or mass spectrometer cracking of the C_4 photofragments. The source of the mass 15 signal was resolved by lowering the photolysis temperature to 157 K (see dashed traces in Fig. 6 which are displaced for ease of viewing). Based on previous work [36,37], *t*-butyl radicals generated by UV irradiation should be trapped on the surface at 157 K. At this temperature, any isobutane molecules formed should desorb since this molecule is unstable on TiO_2(1 1 0) above ~145 K. Isobutene molecules can be retained below ~185 K. The dashed traces in Fig. 6 show that the photodesorption yield of isobutene and *t*-butyl radical decreased relative to the yields at 285 K, while the photodesorption yield of isobutane increased slightly. More significantly, the mass 15 signal was almost completely absent during 157 K irradiation. Because CH_3 radicals are not captured by the surface at 100 K during photolysis of other diolates [15,26], these data suggest that the mass 15 signal was due to cracking of C_4 products and not from methyl radicals produced during UV irradiation of pinacolone diolate on TiO_2(1 1 0). Instead, this diolate photodecomposes selectively through ejection of *t*-butyl radicals and retention of acetate on the surface.

In a final example of selective radical photodesorption from adsorbed organic diolates on TiO_2, Figs. 7 and 8 show photodesorption data from UV irradiation of chloroacetone diolates formed from coadsorption of chloroacetones and oxygen on the TiO_2(1 1 0) surface. Fig. 7 shows photodesorption data from coadsorption of chloroacetone and oxygen. The only detected signals (at masses 47–49) resulted from mass spectrometer cracking fragments attributable to the chloromethyl radical (CH_2Cl). (The contribution at mass 49 from $C^{37}Cl^+$ was removed by subtracting a normalized mass 47 signal obtained using the natural abundances for the Cl isotopes.) Although a mass spectrum of gaseous CH_2Cl radical is not available in the literature, the ratio of mass 49 ($CH_2^{35}Cl^+$) to mass 48 ($CH^{35}Cl^+$) to mass 47 ($C^{35}Cl^+$) observed is not inconsistent with that obtained from other CH_2Cl-containing species [38]. For example, the mass 47:48:49 ratio (the latter corrected for isotopic overlap) from mass spectrometer cracking of CH_3Cl is 0.78:0.37:1, which is close to the 0.67:0.31:1 ratio observed here. Mass 50 is the most intense signal for CH_3Cl. However, no mass 50 signal was observed in the experiments of Fig. 7 (not shown). More significant is the observation that no methyl radical desorption signal was detected (see top of Fig. 8), indicating that hole-mediated photodecomposition of the chloroacetone diolate species occurred selectively through chloromethyl radical ejection. Addition of a second chlorine atom to the starting organic carbonyl (in the form of 1,1-dichloroacetone) did not alter the preference for ejection of the chlorine-containing methyl group over that of the

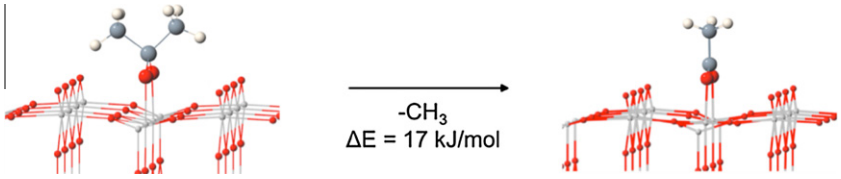

Fig. 9. DFT structures and reaction energy for the conversion of acetone diolate into acetate by the removal of a gas-phase methyl radical.

Table 2
DFT reaction energies for conversion of various carbonyl diolates to carboxylates on TiO_2(1 1 0) by way of ejecting a gas-phase radical of one of the two possible substituents. The middle column shows the absolute value of the energy difference between the two leaving groups, with the arrow pointing toward the theoretically preferred product. Products indicated in bold were observed experimentally. An asterisk indicates that a bound state for these diolate species was not found with DFT.

Parent carbonyl	Leaving group	(kJ/mol)	Difference $\lvert CH_3 - R\rvert$ (kJ/mol)	Leaving group	(kJ/mol)
Acetone	CH_3	17			
Acetaldehyde	CH_3	43	←21	H	64
2-Butanone	CH_3	24	16→	CH_2CH_3	8
Pinacolone[a]	CH_3		?→	$C(CH_3)_3$	≪0
Acetophenone	CH_3	−1	←39	C_6H_5	38
Acetyl chloride	CH_3	10	53→	Cl	−43
1-Chloroacetone	CH_3	41	51→	CH_2Cl	−10
1,1-Dichloroacetone	CH_3	45	81→	$CHCl_2$	−36
1,1,1-Trichloroacetone	CH_3	−6	116→	CCl_3	−122
1,1,1-Trifluoroacetone	CH_3	26	50→	CF_3	−24
Hexafluoroacetone	CF_3	−65			

[a] A bound state for this diolate species was not found with DFT.

non-chlorinate methyl (middle of Fig. 8), but it appeared to significantly decrease the yield of the chlorinated methyl radical ($CHCl_2$ in this case) that was able to escape the surface. Although not shown in Fig. 8, the mass 47:48:49 (corrected) ratio from photodesorption of $CHCl_2$ was 1:0.49:0.05, which is comparable to the 47:48:49 (corrected) ratio for mass spectrometer cracking of $CHCl_2Br$ and $CHCl_2F$ [38]. This comparison suggests that the mass 47 signal should be the more intense of the three for $CHCl_2$ radical, so the weak signal at mass 47 can be interpreted as a low photodesorption yield of $CHCl_2$ radical. A significant change occurred in the fully chlorinating methyl substituent case (i.e., 1,1,1-trichloroacetone) in the form of a redistribution of the ejected radical selectivity to include some methyl (mass 15) as well as some trichloromethyl photodesorption. This is similar to the case of 1,1,1-trifluoroacetone where both CF_3 and CH_3 were detected from photodecomposition of the corresponding diolate [27].

The ability to predict which R group on an organic carbonyl molecule will be photodesorbed, and which will remain on the surface as the carboxylate product, may lie in an energetic understanding of the relative bond energies of the corresponding organic carbonyl diolate species. DFT was used to predict the favored photodecomposition pathway by comparing energies of the initial and final reaction species, for both potential bond breaking events in various adsorbed carbonyl diolates. For example, Fig. 9 shows the energy change for C–CH_3 bond cleavage in acetone diolate, where the starting point was the adsorbed acetone diolate and the end point was a gas-phase CH_3 radical and an adsorbed acetate. The energy for this reaction is close to thermal neutral (∼17 kJ/mol) despite the formation of a gaseous radical. This illustrates the energetic advantage in forming a carboxylate on the surface from the diolate (Fig. 9 and Reaction 3).

$$\eta^2\text{-acetone diolate}_{(a)} \rightarrow CH_{3(g)} + \eta^2\text{-acetate}_{(a)} \quad (3)$$

Table 2 displays reactions energies obtained from DFT for the other organic diolates considered in this study, with values presented for both reaction options (i.e., R_1 and R_2, where $R_1 \neq R_2$). There is general agreement between the selectivities observed experimentally and those calculated with DFT. The exceptions is for pinacolone where a bound diolate was not observed theoretically, and therefore energy differences between the two pathways could not be calculated. Our attempts to converge the surface-bound diolates for this molecule led to radical ejection and formation of the carboxylate, which indicates a strong energetic drive for radical ejection in this case. DFT also predicts for 1,1,1-trifluoroacetone that ejection of a CF_3 radical should take precedence over that of a CH_3 radical (by ∼50 kJ/mol). In the case of pinacolone, the inability of DFT to converge on a stable diolate nevertheless revealed a 'preference'

Table 3
DFT reaction energies for conversion of various carboxylates to CO_2 and a gas-phase radical on TiO_2(1 1 0).

Carboxylate	Leaving group	(kJ/mol)
Acetate	CH_3	198
Benzoate	C_6H_5	237
Formate	H	219
Trifluoroacetate	CF_3	148

Table 4
DFT reaction energies indicating the general stability of the organic radicals considered in this work. The numbers correspond to reaction energies for the reactions: R – H → R + H. Lower energies represent more stable radicals.

R group	(kJ/mol)
H	443
CH_3	457
CH_2CH_3	438
$C(CH_3)_3$	409
C_6H_5	477
Cl	443
CH_2Cl	430
$CHCl_2$	411
CCl_3	397
CF_3	453

for *t*-butyl radical ejection. This ejection pathway is consistent with experiment. We encountered similar difficulty in converging the 1,1,1-trichloroacetone diolate species. For 1,1,1-trichloroacetone, most simulation runs led to CCl_3 ejection and carboxylate formation rather than a stable diolate. Only after careful simulations was the stable adsorbed diolate state obtained. The results in Table 2 illustrate why this occurred; the reaction energy for CCl_3 ejection was very exothermic at −122 kJ/mol. The 1,1,1-trichloroacetone DFT results are consistent with the photodesorption data in that both CH_3 and CCl_3 ejection processes are predicted to be exothermic, while both R groups are observed experimentally. The experimental observation of both R groups does not arise from sequential photochemistry, as shown in Reactions 4 and 5:

$$\eta^2\text{-R}_1,\text{R}_2\text{-diolate}_{(a)} + h\nu \rightarrow \text{R}_{1(g)} + \eta^2\text{-R}_2\text{-carboxylate}_{(a)} \quad (4)$$

$$\eta^2\text{-R}_2\text{-carboxylate}_{(a)} + h\nu \rightarrow \text{R}_{2(g)} + \text{CO}_{2(g)} \quad (5)$$

The photodecomposition of acetate on TiO_2(1 1 0) is extremely slow in the absence of gas-phase O_2 [39], and the same appears to be the case for trifluoroacetate [27]. Table 3 suggests that inactivity for the direct photodecomposition of carboxylates on TiO_2(1 1 0) may be due to reactions that are significantly 'up-hill' energetically speaking. While these values say nothing about the energy of the 'neutralized' carboxylate (i.e., formed immediately after reaction with a valence band hole) or of any reaction barriers, they along with experimental results suggest that energy partitioning in the 'excited' state of these diolates causes fragmentation events that do not necessarily follow what is expected based on thermodynamics.

We can also rationalize the preference for R-group ejection based on the final radical stability. We calculated the stability of the radicals of interest through a series of reactions, as given in Table 4. The general stability ordering of organic radicals is similar to cation stability and follows: tertiary > secondary > primary > phenyl. The stability of the larger hydrocarbons can be explained by their increased ability for charge delocalization of the unpaired electron or by resonance stabilization. In the case of the phenyl group, formation of the radical breaks the aromatic structure, leading to the most unstable radical. Furthermore, radicals are electron-deficit so electron-donating species stabilize the radicals, which explains why the halogen-containing radicals are more stable than their corresponding CH_3 radical. These radical stability calculations are consistent with the preferred ejected radicals given in Table 2, with the exception of the H radical, which may simply indicate that better-formed (isodesmic) reactions may exist, rather than the ones we chose, to describe H radical formation. Nevertheless, the gas-phase radical stability provides a predictive way in most cases of determining photodecomposition pathways of the adsorbed ketones.

4. Conclusions

The use of the ultrahigh vacuum surface science approach and state-of-the-art theoretical methods show that organic radical ejection is an important and potentially commonplace reaction process occurring during photooxidation reactions on TiO_2 surfaces. These radicals are likely short-lived under applied conditions, and thus difficult to detect, but are readily detectable during direct hole-mediated photodecomposition processes on TiO_2 surface in vacuum. Knowledge of the reactants permits use of theoretical methods to predict what bonds are broken and what bonds are retained as a result of photochemical charge transfer processes on TiO_2. With these approaches, it is possible to identify and map out preferred and unfavorable mechanistic pathway during photocatalytic reactions on TiO_2, as we demonstrate for the case of photodecomposition of organic carbonyls on the rutile TiO_2(1 1 0) surface.

Acknowledgments

The authors thank Dave Dixon for his insights. Work reported here was supported by the US Department of Energy, Office of Basic Energy Sciences, Division of Chemical Sciences, Geosciences, and Biosciences. Pacific Northwest National Laboratory is a multiprogram national laboratory operated for the US Department of Energy by the Battelle Memorial Institute under contract DEAC06-76RLO1830. The experimental studies reported here were performed in the William R. Wiley Environmental Molecular Science Laboratory (EMSL), a Department of Energy user facility funded by the Office of Biological and Environmental Research. Computational resources were provided by the Molecular Science Computing Facility located in EMSL and the National Energy Research Scientific Computing Center in Berkeley, CA.

Appendix A. Supplementary material

Supplementary data associated with this article can be found, in the online version, at doi:10.1016/j.jcat.2011.01.021.

References

[1] J.M. Coronado, J. Soria, Catalysis Today 123 (2007) 37–41.
[2] E. Carter, A.F. Carley, D.M. Murphy, ChemPhysChem 8 (2007) 113–123.
[3] A.L. Attwood, J.L. Edwards, C.C. Rowlands, D.M. Murphy, Journal of Physical Chemistry A 107 (2003) 1779–1782.
[4] C.A. Jenkins, D.M. Murphy, Journal of Physical Chemistry B 103 (1999) 1019–1026.
[5] Y. Nosaka, K. Koenuma, K. Ushida, A. Kira, Langmuir 12 (1996) 736–738.
[6] D. Brinkley, T. Engel, Journal of Physical Chemistry B 104 (2000) 9836–9841.
[7] F. Arsac, D. Bianchi, J.M. Chovellon, C. Ferronato, J.M. Herrmann, Journal of Physical Chemistry A 110 (2006) 4213–4222.
[8] F. Arsac, D. Bianchi, J.M. Chovelon, C. Ferronato, J.M. Herrmann, Journal of Physical Chemistry A 110 (2006) 4202–4212.
[9] D. Brinkley, T. Engel, Journal of Physical Chemistry B 102 (1998) 7596–7605.
[10] W.Z. Xu, D. Raftery, Journal of Physical Chemistry B 105 (2001) 4343–4349.
[11] W.Z. Xu, D. Raftery, J.S. Francisco, Journal of Physical Chemistry B 107 (2003) 4537–4544.
[12] D. Brinkley, T. Engel, Surface Science 415 (1998) L1001–L1006.
[13] C.P. Chang, J.N. Chen, M.C. Lu, Journal of Chemical Technology and Biotechnology 79 (2004) 1293–1300.
[14] N. Sakaguchi, S. Matsuo, T. Kurisaki, T. Matsuo, H. Wakita, Research on Chemical Intermediates 32 (2006) 95–101.
[15] M.A. Henderson, Journal of Physical Chemistry B 109 (2005) 12062–12070.
[16] CP2K development home page, 2009. <http://cp2k.berlios.de>.
[17] G. Lippert, J. Hutter, M. Parrinello, Theoretical Chemistry Accounts 103 (1999) 124.
[18] J. Van deVondele, M. Krack, F. Mohamed, M. Parrinello, T. Chassaing, J. Hutter, Computer Physics Communications 167 (2005) 103.
[19] J.P. Perdew, K. Burke, M. Ernzerhof, Physical Review Letters 77 (1996) 3865.
[20] S. Goedecker, M. Teter, J. Hutter, Physical Review B 54 (1996) 1703.
[21] M. Krack, Theoretical Chemistry Accounts 114 (2005) 145.
[22] M.A. Henderson, Journal of Physical Chemistry B 108 (2004) 18932–18941.
[23] M.A. Henderson, Journal of Catalysis 256 (2008) 287–292.
[24] M.A. Henderson, Journal of Physical Chemistry C 112 (2008) 11433–11440.
[25] M.A. Henderson, Surface Science 602 (2008) 3188–3193.
[26] R.T. Zehr, M.A. Henderson, Surface Science 602 (2008) 2238–2249.
[27] R.T. Zehr, N.A. Deskins, M.A. Henderson, Journal of Physical Chemistry C 114 (2010) 16900.
[28] R.T. Zehr, M.A. Henderson, Physical Chemistry Chemical Physics 12 (2010) 8084.
[29] T.-H. Wang, D.A. Dixon, M.A. Henderson, Journal of Physical Chemistry C 114 (2010) 14083.
[30] M.A. Henderson, W.S. Epling, C.L. Perkins, C.H.F. Peden, U. Diebold, Journal of Physical Chemistry B 103 (1999) 5328–5337.
[31] W.S. Epling, C.H.F. Peden, M.A. Henderson, U. Diebold, Surface Science 413 (1998) 333–343.
[32] Y. Du, Z. Dohnalek, I. Lyubinetsky, Journal of Physical Chemistry C 112 (2008) 2649–2653.
[33] Y. Du, N.A. Deskins, Z. Zhang, Z. Dohnalek, M. Dupuis, I. Lyubinetsky, Physical Review Letters 102 (2009) 096102.

[34] Y. Du, N.A. Deskins, Z. Zhang, Z. Dohnalek, M. Dupuis, I. Lyubinetsky, Physical Chemistry Chemical Physics 114 (2010) 17080.
[35] S. Wendt, P.T. Sprunger, E. Lira, G.K.H. Madsen, Z. Li, J.O. Hansen, J. Matthiesen, A. Blekinge-Rasmussen, E. Laegsgaard, B. Hammer, F. Besenbacher, Science 320 (2008) 1755–1759.
[36] J.M. White, M.A. Henderson, Journal of Physical Chemistry B 109 (2005) 12417–12430.
[37] J.M. White, M.A. Henderson, Journal of Physical Chemistry B 109 (2005) 14990–15000.
[38] P.J. Linstrom, W.G. Mallard (Eds.), NIST Chemistry WebBook, NIST Standard Reference Database Number 69, National Institute of Standards and Technology, Gaithersburg, MD, 2010. <http://webbook.nist.gov/chemistry/>.
[39] H. Idriss, P. Legare, G. Maire, Surface Science 515 (2002) 413–420.